PHILOSOPHICAL TRANSACTIONS OF THE ROYAL SOCIETY A

Phil. Trans. R. Soc. A
doi:10.1098/rsta.2009.0232

Review

Delay stabilization of periodic orbits in coupled oscillator systems

By B. Fiedler[1], V. Flunkert[2], P. Hövel[2,*] and E. Schöll[2]

[1]*Institut für Mathematik I, FU Berlin, Arnimallee 2-6, 14195 Berlin, Germany*
[2]*Institut für Theoretische Physik, Technische Universität Berlin, Hardenbergstraße 36, 10623 Berlin, Germany*

We study diffusively coupled Hopf normal form oscillators. By introducing a non-invasive delay coupling, we are able to stabilize the inherently unstable anti-phase orbits. For the super- and subcritical case, we state a condition on the oscillator's nonlinearity which is necessary and sufficient to find coupling parameters for successful stabilization. We prove these conditions and review previous results on the stabilization of odd-number orbits by time-delayed feedback. Finally, we illustrate the results with numerical simulations.

Keywords: delay; stabilization; coupled systems

1. Introduction

Coupled nonlinear oscillators are models for complex systems in different fields of science ranging from engineering to neurology. Understanding and controlling the behaviour of these oscillators is therefore a central issue in nonlinear science.

The control of resonance effects and synchronization is of particular importance. For instance, cognitive brain functions (binding problem) and pathological brain conditions such as epilepsy and Parkinson's disease (Schiff *et al.* 1994; Rosenblum *et al.* 2001; Rosenblum & Pikovsky 2004; Popovych *et al.* 2005) are related to the synchronization of neurons and neural populations. Time delays are always present in coupled systems owing to the finite signal propagation time. These time lags give rise to complex dynamics and have been shown to play a key role in the synchronization behaviour of neural systems (Hauschildt *et al.* 2006; Gassel *et al.* 2007; Dahlem *et al.* 2009; Schöll *et al.* 2009). Coupled lasers exhibit similar phenomena as coupled neurons and have attracted much attention owing to their importance in telecommunication application (Wünsche *et al.* 2005; Fischer *et al.* 2006; Klein *et al.* 2006; Shaw *et al.* 2006; Landsman & Schwartz 2007; Flunkert *et al.* 2009). For many technological and medical applications, non-invasive methods of control are desirable as they have no side effects and do not compromise the performance of the controlled system. On the other hand, non-invasive control methods also provide an effective tool for

*Author for correspondence (phoevel@physik.tu-berlin.de).

One contribution of 13 to a Theme Issue 'Delayed complex systems'.

studying complex systems because they allow us to uncover unstable dynamical structures in experiments (Sieber *et al.* 2008). Stabilization of unstable periodic orbits has thus been identified as a task of central importance, even in the context of chaotic dynamics (Ott *et al.* 1990; Boccaletti *et al.* 2000; Gauthier 2003; Schöll & Schuster 2008). *Delayed feedback* control as proposed by Pyragas (1992) has proven to be a powerful non-invasive method for the stabilization of unstable periodic orbits (Schöll & Pyragas 1993; Baba *et al.* 2002; Beck *et al.* 2002; von Loewenich *et al.* 2004) and unstable steady states (Hövel & Schöll 2005; Schikora *et al.* 2006; Dahms *et al.* 2007, 2008) in dynamical systems. It has for instance been successfully applied in spatially extended systems (Unkelbach *et al.* 2003; Stegemann *et al.* 2006; Postlethwaite & Silber 2007; Dahlem *et al.* 2008, in press; Schneider *et al.* 2009; Kyrychko *et al.* submitted) and even in noise driven-systems (Janson *et al.* 2004; Pomplun *et al.* 2005; Flunkert & Schöll 2007; Prager *et al.* 2007; Pototsky & Janson 2007; Hizanidis & Schöll 2008; Majer & Schöll 2009).

The basic idea is as simple, as it is often effective. Let $z = z(t) = z(t + p)$, $t \in \mathbb{R}, z \in \mathbb{R}^n$, denote a periodic orbit with minimum period $p > 0$ of a system,

$$\dot{z} = F(z). \tag{1.1}$$

Then, consider a linear time-delayed feedback

$$\dot{z}(t) = F(z(t)) + B(z(t - \tau) - z(t)), \tag{1.2}$$

involving a time delay $\tau > 0$. For delays $\tau = np$ which are an integer multiple n of the minimum period p, any control force $B(z(t - \tau) - z(t))$ vanishes along the given periodic orbit $z(t)$. The instability of $z(t)$ in equation (1.1), however, may change and may in fact be overcome for suitable choices of the control matrix B in equation (1.2) (Fiedler *et al.* 2007).

The above idea can be implemented and tested easily in experimental systems, even in the absence of specific models $F(z)$. It is therefore perhaps not surprising that the literature on this Pyragas method has grown to about 1000 publications, meanwhile. For some recent surveys on theoretical and experimental aspects, see, for example, Schöll & Schuster (2008).

Severe restrictions for the applicability of the method were believed to exist (Just *et al.* 1997; Nakajima 1997; Nakajima & Ueda 1998*a*; Harrington & Socolar 2001; Pyragas *et al.* 2004; Pyragas & Pyragas 2006). It was commonly believed that unstable periodic orbits with an odd number of real Floquet multipliers larger than unity could never be stabilized by delayed feedback control. Recently, this alleged *odd-number theorem* has been refuted by a counter example (Fiedler *et al.* 2007, 2008*a*,*b*,*c*; Just *et al.* 2007; Kehrt *et al.* 2009) (see §4 for a summary of these results).

In this paper, we study two coupled Hopf normal form oscillators. We generalize the delayed feedback control of Pyragas to a delay coupling in order to stabilize in-phase and anti-phase periodic orbits in the coupled system and thus control specific prescribed synchronization patterns of the oscillators. For anti-phase solutions, we advocate a suitable half-period delayed feedback, which is analogous to a suggestion made by Nakajima & Ueda (1998*b*) in the context of single Duffing and Lorenz equations. To be specific, and to enable complete analytical results, we consider planar oscillators with an additional rotational equivariance; see equation (2.2). Such planar truncated Stuart–Landau

oscillators are mathematically motivated and justified by normal form analysis. In particular, our claims remain valid under perturbations breaking the rotational normal form symmetry and, as well, under perturbations by higher-order terms.

This paper is organized as follows. In §2, we introduce the model of two diffusively coupled Hopf normal form oscillators and investigate the in-phase and anti-phase solutions. Section 3 describes our non-invasive delay coupling and states the stabilization theorems—the main results of this work. In §4, we review previous results on the stabilization of *subcritical* Hopf bifurcation, in planar normal form, by non-invasive delayed feedback as a preparation for the proofs of the theorems. Section 5 discusses the characteristic equation of our control system (3.2), linearized at $z_1 = z_2 = 0$. Section 6 proves the theorems formulated in §3. In §7, we provide some numerical illustration. Finally, §8 concludes with a discussion of our results.

2. Model of two diffusively coupled oscillators

Our model system (1.1) takes the following specific form:

$$\dot{z}_1 = f(z_1) + a \cdot (z_2 - z_1) \tag{2.1a}$$

and

$$\dot{z}_2 = f(z_2) + a \cdot (z_1 - z_2). \tag{2.1b}$$

Here, the planar vectors $z_1, z_2 \in \mathbb{R}^2 \cong \mathbb{C}$ describe the state of the respective oscillator, and

$$f(z) = (\lambda + i + \gamma |z|^2) z \tag{2.2}$$

with real parameter λ and fixed complex γ describes the nonlinear dynamics of each separate oscillator. Note that $f(z)$ is chosen to coincide with the normal form for Hopf bifurcation, truncated at third order. The angular frequency at the Hopf bifurcation is normalized to unity. The scalar $a > 0$ is the diffusive coupling constant. The individual oscillator z_i undergoes Hopf bifurcation of a periodic orbit

$$z_1(t) = z_2(t) = z_+(t) = r_+ \exp\left(\frac{2\pi i t}{p_+}\right) \tag{2.3}$$

with amplitude $r_+^2 = -\lambda / Re\,\gamma$ for $\lambda\, Re\,\gamma < 0$, as λ increases through the bifurcation point $\lambda = 0$. The Hopf bifurcation is subcritical for fixed $Re\,\gamma > 0$, and *supercritical* for $Re\,\gamma < 0$. The minimum period p_+ depends on the amplitude r_+ via

$$\frac{2\pi}{p_+} = 1 + r_+^2\, \mathrm{Im}\gamma. \tag{2.4}$$

Owing to symmetry, the coupled oscillator dynamics (2.1) possesses dynamically invariant subspaces. Let

$$z_\pm = \tfrac{1}{2}(z_1 \pm z_2) \tag{2.5}$$

denote the average and the asynchrony of the two oscillators. Then,

$$\dot{z}_+ = \tfrac{1}{2}\,(f\,(z_+ + z_-) + f\,(z_+ - z_-)) \tag{2.6a}$$

and

$$\dot{z}_- = \tfrac{1}{2}\,(f\,(z_+ + z_-) - f\,(z_+ - z_-)) - 2az_- \tag{2.6b}$$

is equivalent to equations (2.1). Note how $\dot{z}_- = 0$ for $z_- = 0$; hence, the *in-phase subspace*

$$Z_+ := \{(z_+, z_-) | z_- = 0\}, \tag{2.7}$$

characterized by $z_1 \equiv z_2$ is dynamically invariant. Because $f(-z) = -f(z)$ is an odd nonlinearity, the *anti-phase* subspace

$$Z_- = \{(z_+, z_-) | z_+ = 0\}, \tag{2.8}$$

where $z_1 \equiv -z_2$, is likewise invariant.

Specifically, the in-phase dynamics on Z_+ coincides with equation (2.2) and features Hopf bifurcation of the periodic orbit $z_+(t)$ with minimum period p_+ as in equations (2.3) and (2.4). The anti-phase dynamics on Z_-, by contrast, is given by

$$\dot{z}_- = f(z_-) - 2az_-. \tag{2.9}$$

Therefore, anti-phase Hopf bifurcation occurs at $\lambda = 2a$ and generates periodic orbits

$$z_-(t) = r_- \exp\left(\frac{2\pi\, it}{p_-}\right), \tag{2.10}$$

with amplitude $r_-^2 = -(\lambda - 2a)/Re\,\gamma$ and minimum period p_- according to

$$\frac{2\pi}{p_-} = 1 + r_-^2\,\mathrm{Im}\,\gamma. \tag{2.11}$$

Compared with in-phase Hopf bifurcation at $\lambda = 0$, the anti-phase Hopf bifurcation point $\lambda = 2a$ has shifted to the right, by $2a$, but the bifurcation direction coincides with the in-phase solutions. Indeed, the dynamics in Z_+ and Z_- only differ by a shift of $2a$ in the bifurcation parameter λ.

The above elementary observations have an important consequence for the stability properties of the bifurcating anti-phase periodic orbits $z_-(t)$. As $\lambda = 2a > 0$, at Hopf bifurcation, the unstable dimension of $z_-(t)$ is at least 2, as inherited from the Hopf bifurcation point itself. Specifically, the unstable dimension is 3 in the subcritical case $Re\,\gamma > 0$, and 2 in the supercritical case $Re\,\gamma < 0$. As usual, the unstable dimension denotes the number of Floquet multipliers strictly outside the complex unit circle, counting algebraic multipliers. See Diekmann *et al.* (1998), Schöll & Schuster (2008), Fiedler *et al.* (2007) and Just *et al.* (2007) for the mathematical centre manifold machinery behind this result on exchange of stability at bifurcations. See also figure 1.

3. Stabilization by delay—theorems

We now attempt to stabilize the unstably born anti-phase periodic solution $z_-(t)$ by a delayed control term that is adapted to the specific symmetry $z_+ \equiv 0$ of $z_-(t)$. Recall that $z_-(t - p_-/2) = -z_-(t)$; see equation (2.10). Therefore, $z_+ \equiv 0$

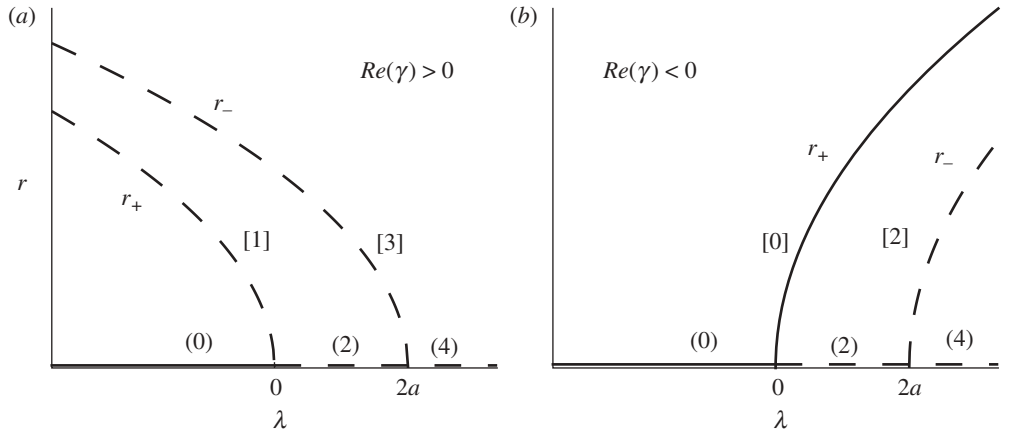

Figure 1. In-phase (r_+) and anti-phase (r_-) Hopf bifurcation of periodic orbits $z_\pm(t)$. Dashed/solid curves denote instability/stability. (a) and (b) show the subcritical and supercritical cases, respectively. Unstable dimensions are indicated in parentheses, for the trivial equilibrium $z \equiv 0$, and in brackets, for the bifurcating periodic orbits.

implies the following spatio-temporal symmetry with respect to exchanging the two subsystems

$$z_1(t) = z_2\left(t - \frac{p_-}{2}\right) \tag{3.1a}$$

and

$$z_2(t) = z_1\left(t - \frac{p_-}{2}\right). \tag{3.1b}$$

Indeed, the oscillators switch their roles after half a period, in the anti-phase case. This in turn motivates us to seek a stabilization of the solution $z_-(t)$ in the form of delayed coupling

$$\dot{z}_1 = f(z_1) + a \cdot (z_2 - z_1) + b \cdot (z_2(t-\tau) - z_1) \tag{3.2a}$$

and

$$\dot{z}_2 = f(t_2) + a \cdot (z_1 - z_2) + b \cdot (z_1(t-\tau) - z_2) \tag{3.2b}$$

for complex parameter $b \in \mathbb{C}$. Omitted arguments of z_1, z_2 indicate evaluation at time t here. Note that the delay τ is non-invasive for

$$\tau = \tfrac{1}{2} n p_-, \tag{3.3}$$

Q3 i.e. for integer multiples n of *half* the minimum period p_-. Such a delayed coupling would be invasive on in-phase solutions z_+, because $z_2(t-\tau) - z_1(t) = z_1(t-\tau) - z_2(t) \neq 0$, for half-period delays τ, unless $p_+ = p_-/2$.

Next, we state stabilization theorems for the supercritical and subcritical cases. The respective proofs follow in §6.

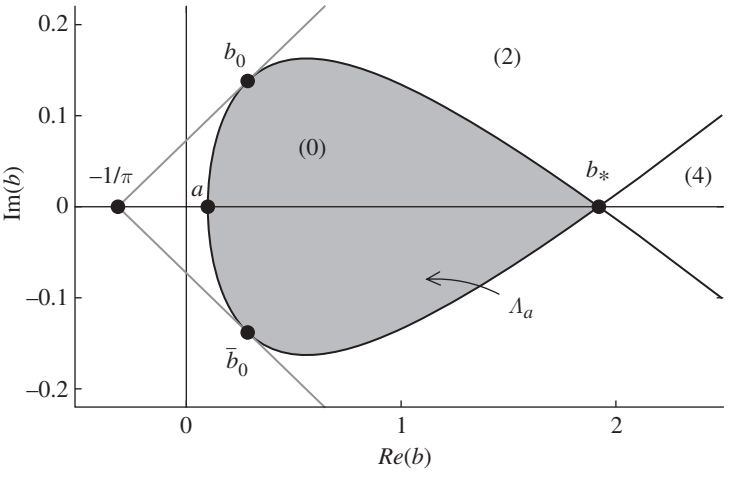

Figure 2. Stabilization region Λ_a (shaded) of complex control coefficients $b \in \mathbb{C} \setminus \mathbb{R}$ for anti-phase solutions near supercritical Hopf bifurcation. The numbers in parentheses indicate the total multiplicity $E(b)$ of eigenvalues with strictly positive real part, at Hopf bifurcation $\lambda = 2a$. Note that straight lines through $b = -1/\pi \in \mathbb{C}$ touch the boundary of Λ_a in the points b_0 and $\bar{b}_0$ (see §6). Parameter: $a = 0.1$.

Theorem 3.1. *Consider the coupled oscillator systems (2.1) and (2.2) with diffusive coupling constant*

$$0 < a < \frac{1}{\pi}, \tag{3.4}$$

in the supercritical case $Re\,\gamma < 0$. Then, there exists a strictly decreasing real analytic function $b_* = b_*(a) > a$ with limits $b_*(0) = \infty$ and $b_*(1/\pi) = 1/\pi$ such that for real controls

$$a < b < b_*(a) \tag{3.5}$$

the anti-phase periodic orbits $z_-(t) \not\equiv 0, z_+ \equiv 0$ of equations (2.10) and (2.11) are stabilized non-invasively by a delayed coupling (3.2) with half-period delay

$$\tau = \tfrac{1}{2} p_-, \tag{3.6}$$

for small amplitudes $r_- = |z_-(t)|$, and for parameters λ near the anti-phase Hopf bifurcation at $\lambda = 2a$.

Theorem 3.2. *Consider the subcritical case $Re\,\gamma > 0$ of theorem 3.1, again for $0 < a < 1/\pi$. Then, there exists a continuous, strictly increasing function $\beta = \beta(a)$ with limits $\beta(0) > 0$ and $\beta(1/\pi) = \infty$ such that the following holds for*

$$|\mathrm{Im}\,\gamma| > \beta(a)\, Re\,\gamma. \tag{3.7}$$

For each pair of a, γ satisfying equation (3.7), there exists an open region of controls $b \in \mathbb{C}\setminus\mathbb{R}$, depending on a and γ, for which equations (3.2) achieve non-invasive delayed feedback stabilization locally near Hopf bifurcation at $\lambda = 2a$, as asserted in theorem 3.1.

See figure 2 for a sketch of the stabilization regime $b \in \mathbb{C}\setminus\mathbb{R}$ to which theorem 3.2 applies. The shaded region Λ_a indicates the region of those strictly complex controls b for which stabilization is possible, locally near anti-phase Hopf

bifurcation, provided that $|\mathrm{Im}\,\gamma|/|Re\,\gamma|$ is large enough. For decreasing values $|\mathrm{Im}\,\gamma|/|Re\,\gamma| \searrow \beta(a)$, the regime of stabilizing b shrinks to two complex conjugate boundary points $b_0(a), \overline{b_0(a)}$. See §5 for details on $b_*(a)$ and the end of §6 for $b_0(a), \beta(a)$. See §7 for numerical examples.

4. Beyond odd-number limitation for planar Hopf bifurcation

As a preparation for the proof of theorems 3.1 and 3.2 in §6, we revisit delayed feedback stabilization of planar Hopf bifurcation in a single system,

$$\dot{z} = f(z) + b \cdot (z(t-\tau) - z), \tag{4.1}$$

with the same normal form nonlinearity $f(z) = (\lambda + i + \gamma|z|^2)z \in \mathbb{C}$ as in equation (2.2). See also Schöll & Schuster (2008), Fiedler *et al.* (2007) and Just *et al.* (2007) for our previous analysis of this case.

Of course, we keep in mind that equation (4.1) also describes stabilization within the invariant subspace $Z_+ = \{(z_1, z_2)|z_- = 0\}$ of the in-phase solutions $z_1(t) \equiv z_2(t)$, introduced in equations (2.5) and (2.7), under the naive delayed feedback control scheme

$$\dot{z}_1 = f(z_1) + a(z_2 - z_1) + b \cdot (z_1(t-\tau) - z_1)\,, \tag{4.2a}$$

and

$$\dot{z}_2 = f(z_2) + a(z_1 - z_2) + b \cdot (z_2(t-\tau) - z_2)\,. \tag{4.2b}$$

We comment on this case in the discussion (§8).

Theorem 4.1. *Consider the planar Hopf normal form system (4.1) with subcritical Hopf bifurcation in the absence of control $b = 0$, i.e. with*

$$Re\,\gamma > 0. \tag{4.3}$$

Then, there exist complex control gains b such that the bifurcating periodic orbits $z(t) = r\exp(2\pi\, it/p), r^2 = -\lambda/Re\,\gamma, p = 2\pi/(1 - \lambda\,\mathrm{Im}\,\gamma/Re\,\gamma)$ are stabilized non-invasively by a delayed feedback (4.1) with delay equal to the period

$$\tau = p. \tag{4.4}$$

This holds for small amplitudes r and for parameters λ near Hopf bifurcation at $\lambda = 0$.

In the absence of control, $b = 0$, the bifurcating periodic solutions $z(t)$ are one-dimensionally unstable. Their stabilization by non-invasive delayed feedback therefore refutes the so-called '*odd-number limitation*' of Pyragas control. See Fiedler *et al.* (2007) and Just *et al.* (2007) for a detailed discussion of this aspect, including rigorous mathematical analysis illustrated by numerical examples.

To prepare for our proof of theorems 3.1 and 3.2 in §§3 and 4, we now sketch a proof of theorem 4.1, in the same spirit. For brevity, we only consider the *hard spring case*,

$$\mathrm{Im}\,\gamma > 0, \tag{4.5}$$

where period $p = 2\pi/(1 + r^2\,\mathrm{Im}\,\gamma)$ decreases with amplitude r, leaving the opposite *soft spring case* $\mathrm{Im}\,\gamma < 0$ to the reader.

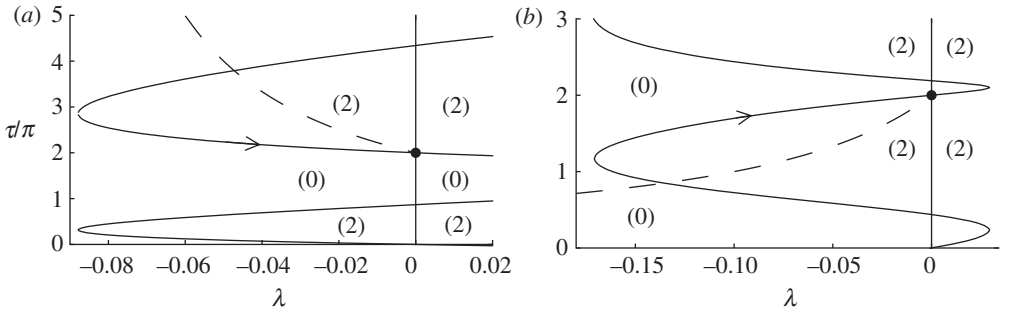

Figure 3. Subcritical Hopf bifurcation in the parameter plane (λ, τ) with fixed control b for (a) soft springs $\mathrm{Im}\,\gamma < 0$ and (b) hard springs $\mathrm{Im}\,\gamma > 0$. Solid black lines display the Hopf bifurcation curve $(\lambda(\omega), \tau(\omega))$ emanating from $\lambda = 0$ and non-invasive delay $\tau = 2\pi$. Hopf curves are oriented with increasing ω. The dashed black lines correspond to the period $\tau = p(\lambda)$ of the Pyragas curve of bifurcating periodic solutions. Strict unstable dimensions $E(b)$ of the trivial equilibrium $z \equiv 0$ are indicated in parentheses. Parameters: (a) (soft spring): $Re\,\gamma = 1, \mathrm{Im}\,\gamma = -10, b = 0.3\,\mathrm{e}^{\mathrm{i}\pi/4}$; (b) (hard spring): $Re\,\gamma = 1, \mathrm{Im}\,\gamma = 10,\ b = 0.1\,\mathrm{e}^{-\mathrm{i}3\pi/4}$.

The mechanical terminology 'soft' and 'hard' spring arises from the pendulum equation $\ddot{x} + D\,x = 0$ with nonlinear spring constant $D = D(x)$. For 'soft' springs $D(x)$, where $D(x)$ decreases with increasing $|x|$, minimal period increases with amplitude. Examples are mathematical pendula $D(x) = \sin x$, or rubber balloons. For 'hard' springs, $D(x)$ increases with $|x|$ and the period decreases with amplitude.

The basic idea of the proof is easily sketched in the two parameter diagram of figure 3. There are two ingredients. *First*, we linearize at the equilibrium $z \equiv 0$ and study the *strict* unstable dimensions. Let $E(b)$ denote the total number of eigenvalues η with $Re\,\eta > 0$, counting real multiplicities. Even for fixed non-zero b, these numbers still depend on (λ, τ) as indicated in figure 3 in parentheses. *Second*, we evaluate the dashed period curve,

$$\tau = p = p(\lambda) = \frac{2\pi}{(1 - \lambda\,\mathrm{Im}\,\gamma/Re\,\gamma)} \tag{4.6}$$

of non-invasive control in figure 3, as it emanates from the Hopf point $\lambda = 0$, $\tau = 2\pi$ to the subcritical side $\lambda < 0$.

With these two ingredients, the proof works as follows. Suppose we can choose b such that the dashed period curve enters a region with $E(b) = 2$ at $\lambda = 0, \tau = 2\pi$, transversely to the Hopf curve and pointing away from the $E(b) = 0$ region, then the subcritical Hopf bifurcation along the λ-axis $\tau = 0$ (alias $b = 0$) has become supercritical for the chosen parameters along the dashed curve. Hence, the bifurcating unstable orbits, for $\tau = 0$, alias $b = 0$, have become stable along the dashed curve of non-invasive delayed feedback control, by standard exchange of stability at Hopf bifurcation.

Let us implement the above idea for our specific case (4.1). Linearization at $z \equiv 0$ yields the characteristic equation

$$0 = \chi(\eta) = \lambda + i + b(\mathrm{e}^{-\tau\eta} - 1) - \eta \tag{4.7}$$

for the eigenvalues η.

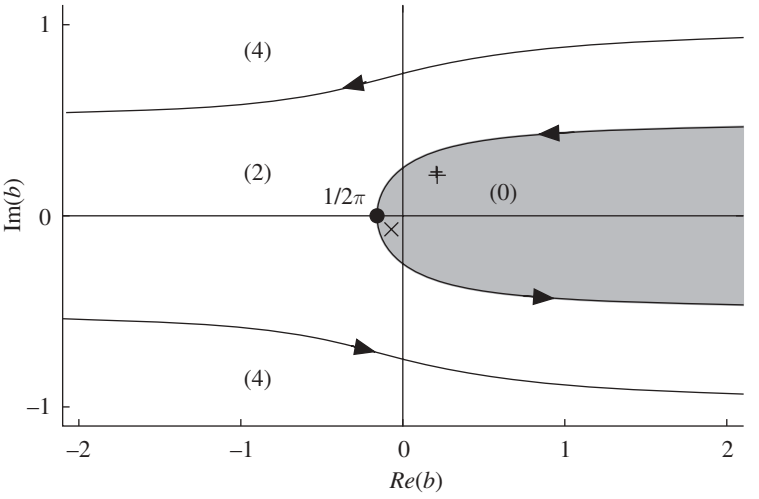

Figure 4. Hopf bifurcation curves $b = b(\omega)$ (solid) and, in parentheses, strict unstable dimensions $E(b)$ at $\lambda = 0, \tau = 2\pi$. Orientation arrows indicate increasing ω. Note the shaded region where $E(b) = 0$. The '+' and '×' mark the values of b for figure 3*a*,*b*, respectively.

First, consider the starting point $\lambda = 0,\ \tau = 2\pi$ with purely imaginary eigenvalue $\eta = i$. We determine the strict unstable dimension $E(b)$ there, aiming for $E(b) = 0$ to ensure that the Hopf eigenvalue $\eta = i$ actually effects a change from $E = 0$ to $E = 2$. Indeed, any $E > 0$ at that starting point, i.e. the presence of any non-Hopf eigenvalues with strictly positive real part, would be inherited as an instability of any bifurcating periodic orbit, obstructing stabilization. Note here that the Hopf eigenvalue pair $\eta = \pm i$ itself does not yet contribute to the strict unstable dimension $E(b)$ at $\lambda = 0$, $\tau = 2\pi$.

At $\lambda = 0, \tau = 2\pi$, the characteristic equation for $\eta = \tilde{\omega} i =: (1 + \omega) i$ reads

$$b = b(\omega) = \frac{i\omega}{\mathrm{e}^{-2\pi i\omega} - 1} = -\frac{\omega}{2}\left(\cot(\pi\omega) + i\right). \tag{4.8}$$

Note $b(0) = -1/(2\pi)$ and the singularities of $b(\omega)$ at integer $\omega \in \mathbb{Z}\backslash\{0\}$. In particular, $\eta = 0$ is never an eigenvalue at $\lambda = 0,\ \tau = 2\pi$, and $E = E(b)$ can only change by Hopf bifurcation there.

As $E(0) = 0$ at $b = 0$, by planarity and the eliminated trivial Hopf eigenvalue $\eta = i$, the strict unstable dimensions $E(b)$ are as indicated in figure 4. Indeed, complex analytic maps, like $\omega \mapsto b(\omega)$, preserve orientation. Instability $E(b)$ tracks eigenvalues $Re\,\eta > 0$ to the right of the imaginary axis $\eta = i\tilde{\omega} = i(1 + \omega)$. Therefore, $E(b)$ is larger by two on the right side of any of the oriented curves $\omega \mapsto b(\omega)$, when compared with the left side. Elsewhere, $E(b)$ does not change. Therefore, all unstable dimensions $E(b)$ in figure 4 follow from $E(0) = 0$ and the indicated orientations of the solid Hopf curves $\omega \mapsto b(\omega)$ for real ω.

We calculate the tangent $\lambda = \hat{\lambda}, \tau = 2\pi + \hat{\tau}$ to the dashed periodic curve $\tau = p(\lambda)$ shown in figure 3. Expanding the explicit representation (4.6),

we immediately obtain

$$\hat{\tau} = 2\pi \frac{\operatorname{Im}\gamma}{Re\,\gamma}\hat{\lambda}. \tag{4.9}$$

To compute the tangent $\lambda = \tilde{\lambda}, \tau = 2\pi + \tilde{\tau}$ to the solid Hopf curve $\lambda = \lambda(\omega)$, $\tau = \tau(\omega)$ of solutions $\eta = i\tilde{\omega} = i(1+\omega)$ at $\omega = 0$, we linearize the characteristic equation (4.7), for fixed b, keeping in mind that $\tilde{\lambda}$ and $\tilde{\tau}$ are of the order ω. Thus, we obtain $0 = \tilde{\lambda} + b(-2\pi i\omega - i\tilde{\tau}) - i\omega$ and the tangent of the Hopf curve

$$\tilde{\lambda} = \frac{\operatorname{Im} b}{Re\, b}\omega \tag{4.10a}$$

and

$$\tilde{\tau} = -\frac{1 + 2\pi\, Re\, b}{Re\, b}\omega. \tag{4.10b}$$

To achieve the geometric hard spring situation shown in figure 3*a*, and hence prove theorem 4.1 in the hard spring case, we recall that both $Re\,\gamma$ and $\operatorname{Im}\gamma$ are positive; see equations (4.3) and (4.5). Hence equation (4.9) makes the slope of the dashed periodic curves positive, in figure 3. By equations (4.10), the slope of the solid Hopf curve, by contrast, is given by

$$\tilde{\tau} = -\frac{1 + 2\pi\ Re\, b}{\operatorname{Im} b}\tilde{\lambda}. \tag{4.11}$$

We now determine the strict unstable dimensions $E(b)$ resulting from different sides of the Hopf curve $\eta = i\tilde{\omega}$ of the characteristic equation (4.7), for fixed b and in the (λ, τ) plane. It is advisable to proceed here with analytic care. Let $(\check{\lambda}, \check{\tau}, \check{\eta}) \in \mathbb{R}^2 \times \mathbb{C}$ denote infinitesimal variations of (λ, τ, η). By multivariate linearization of equation (4.7) at (λ, τ, η), we obtain the equivalent system

$$\varphi(\check{\lambda}, \check{\tau}) := \check{\lambda} - \eta b\, \mathrm{e}^{-\tau\eta}\check{\tau} = \check{\zeta} \tag{4.12a}$$

and

$$\psi(\check{\eta}) := (1 + \tau b\, \mathrm{e}^{-\tau\eta})\check{\eta} = \check{\zeta} \tag{4.12b}$$

with real linear maps $\varphi : \mathbb{R}^2 \to \mathbb{C}$ and $\psi : \mathbb{C} \to \mathbb{C}$. In other words,

$$\check{\eta} \mapsto (\check{\lambda}, \check{\tau}) = (\varphi^{-1} \circ \psi)(\check{\eta}), \tag{4.13}$$

if we eliminate the dummy variable $\check{\zeta} \in \mathbb{C}$.

The map ψ preserves real orientation, being just a multiplication by $1 + \tau b\, \mathrm{e}^{-\tau\eta} \in \mathbb{C}$, for non-zero $1 + \tau b\, \mathrm{e}^{-\tau\eta}$. The map φ, however, when viewed as a linear map $\varphi : \mathbb{R}^2 \to \mathbb{C} \cong \mathbb{R}^2$ by $Re\,\varphi$ and $\operatorname{Im}\varphi$ possesses determinant

$$\begin{aligned} \det\varphi &= -\operatorname{Im}(\eta b\, \mathrm{e}^{-\eta\tau}) \\ &= -\tilde{\omega}(Re(b)\cos(\tilde{\omega}\tau) + \operatorname{Im}(b)\sin(\tilde{\omega}\tau)) \\ &= -Re\, b, \end{aligned} \tag{4.14}$$

at the point of interest $\eta = i\tilde{\omega}, \tilde{\omega} = 1, \lambda = 0, \tau = 2\pi$. In particular, φ preserves orientation for $Re\, b < 0$ as chosen in figure 3*b*. Therefore $\varphi^{-1} \circ \psi$ also preserves orientation in this case.

By equations (4.10) and $\mathrm{Im}\, b < 0$, the Hopf curve is oriented to the upper right at $\lambda = 0, \tau = 2\pi$, as indicated in figure 3*b*. Because $\varphi^{-1} \circ \psi$ from equation (4.13) preserves orientation, $E(b) = 2$ again holds to the right of the oriented Hopf curve $\omega \mapsto (\lambda(\omega), \tau(\omega))$, and the strict unstable dimensions of figure 3*b* follow. The stabilizing condition for the dashed curve $\tau = p(\lambda)$ of the Pyragas periodic orbits (Fiedler *et al.* 2007) to enter the $E(b) = 2$ region when emanating from $\lambda = 0$, $\tau = 2\pi$ to the lower left therefore reads

$$2\pi \frac{\mathrm{Im}\, \gamma}{Re\, \gamma} = \frac{\hat{\tau}}{\hat{\lambda}} > \frac{\tilde{\tau}}{\tilde{\lambda}} = -\frac{1 + 2\pi\, Re\, b}{\mathrm{Im}\, b}. \tag{4.15}$$

Clearly, this can always be achieved in any subcritical, soft spring case of positive $Re\, \gamma$ and $\mathrm{Im}\, \gamma$, if we choose $1 + 2\pi\, Re\, b > 0$ small enough with $Re\, b \gtrsim -1/2\pi$, and $\mathrm{Im}\, b < 0$ also negative, such that b resides in the lower left part of the shaded region indicated in figure 4.

We have thus achieved supercritical Hopf bifurcation along the dashed line of non-invasive delayed feedback in figure 3, and hence local stability of the bifurcating branch. This proves theorem 4.1.

5. Characteristic equations for two coupled oscillators

In this section, we return to our control system (3.2) of coupled oscillators, linearized at $z_1 \equiv z_2 \equiv 0$. In terms of the coordinates $z_\pm = (z_1 \pm z_2)/2$ from equation (2.5), the linearization reads

$$\dot{z}_+ = (\lambda + i) z_+ + b \cdot (z_+(t - \tau) - z_+), \tag{5.1a}$$

and

$$\dot{z}_- = (\lambda - 2a + i) z_- - b \cdot (z_-(t - \tau) + z_-). \tag{5.1b}$$

Note how the linearization decouples into $Z_\pm$ components $z_\pm$, just as in the case $b = 0$ of absent control; see equations (2.5)–(2.11). In the previous section, non-invasive delay stabilization of local subcritical Hopf bifurcation was achieved once that Hopf point itself was stabilized. Analogously, we now study stability at the Hopf point $\lambda = 2a$ itself, before addressing the bifurcating anti-phase orbits in the following section.

The exponential ansatz $z_\pm = \exp(\eta t)$ yields the following two characteristic equations:

$$0 = \chi_+(\eta) = \lambda + i + b(\mathrm{e}^{-\tau\eta} - 1) - \eta, \tag{5.2a}$$

and

$$0 = \chi_-(\eta) = \lambda - 2a + i - b(\mathrm{e}^{-\tau\eta} + 1) - \eta. \tag{5.2b}$$

Because the linearization equations (5.1) decouple in $z_\pm$, each of equations (5.2) contributes its own independent set of eigenvalues to the total spectrum; the strict unstable dimensions $Re\,\eta > 0$ of χ_+ and χ_- therefore add up to the total unstable dimension $E(b) = E_+(b) + E_-(b)$ of the trivial equilibrium, see equation (5.8).

Our analysis of equations (5.2) does not aim at solving these equations for their complex roots η, for example, by tools like the Lambert function. Instead, we are interested in the stability boundary in the space of the five parameters a, $Re\,\gamma$, $\mathrm{Im}\,\gamma$, $Re\,b$ and $\mathrm{Im}\,b$. For this purpose, we will insert $\eta = i\tilde{\omega}$ in equation (5.7) below and study the resulting Hopf curves in the complex b plane, with parameters a, $Re\,\gamma$ and $\mathrm{Im}\,\gamma$.

For $b = 0$, we find a Hopf bifurcation in $Z_- = \{(z_+, z_-) | z_+ = 0\}$ at $\lambda = 2a$ and $\eta = i$, i.e. for period $p_- = 2\pi$. Therefore, $\tau = p_-/2 = \pi$ at the Hopf bifurcation and equations (5.2) become

$$0 = \chi_+(\eta) = 2a + i + b(\mathrm{e}^{-\pi\eta} - 1) - \eta, \tag{5.3a}$$

and

$$0 = \chi_-(\eta) = i - b(\mathrm{e}^{-\pi\eta} + 1) - \eta. \tag{5.3b}$$

First, consider $b = 0$. The complex notation which we have employed then provides a single eigenvalue $\eta = 2a + i$ with positive real part in $Z_+ = \{(z_+, z_-) \mid z_- = 0\}$ from equation (5.3a). In Z_-, the characteristic equation (5.3b) provides the simple Hopf eigenvalue $\eta = i$, as expected. Let $E(b)$ again denote the total number of eigenvalues η with $Re\,\eta > 0$, adding both Z_+ and Z_- and counting real multiplicities. Then, we have just proved

$$E(0) = 2, \tag{5.4}$$

at $\lambda = 2a, \tau = \pi$, for this strict unstable (or expanding) dimension $E(b)$.

Could the unstable dimension $E(b)$ change, as b varies? To achieve our goal

$$E(b) = 0, \tag{5.5}$$

of Hopf stabilization at $\lambda = 2a, \tau = \pi$, it better changes, somehow.

We first note $E(b) = 2$ for small $|b|$. Indeed, the delay exponential $\exp(-\pi\eta)$ then just generates a plethora of countably infinitely many discrete eigenvalues η, in each of the characteristic equations (5.3), all with large negative real part.

Can $E(b)$ change by an eigenvalue η crossing zero as b varies? Inserting $\eta = 0$ in equations (5.3) shows that this cannot happen via χ_+. In χ_-, however, $\eta = 0$ is a solution if and only if,

$$b = \frac{i}{2}. \tag{5.6}$$

It remains to study the changes of $E(b)$ by a purely imaginary Hopf eigenvalue

$$\eta = i\tilde{\omega}. \tag{5.7}$$

Let $E_\pm(b)$ count the solutions η with $Re\,\eta > 0$ of $\chi_\pm(\eta) = 0$, with algebraic multiplicity, so that

$$E(b) = E_+(b) + E_-(b). \tag{5.8}$$

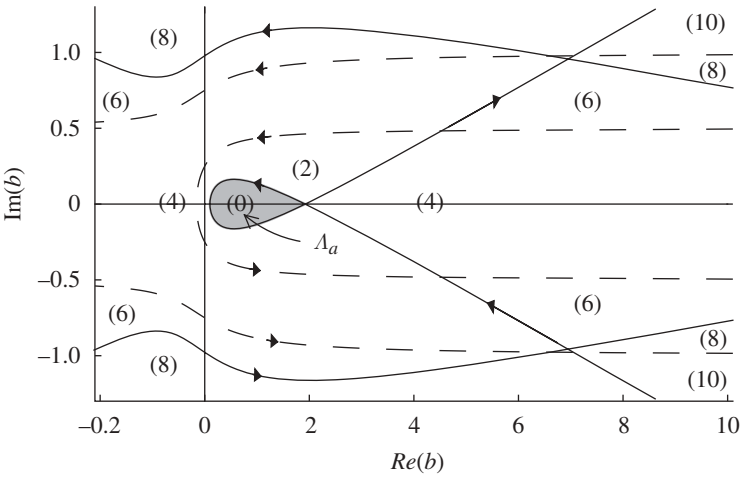

Figure 5. Oriented Hopf curves $b = b_+(\omega)$, solid, and $b = b_-(\omega)$, dashed, for $\omega \in \mathbb{R}$ in control system (3.2), linearized at $z_1 \equiv z_2 \equiv 0$. Orientation arrows indicate increasing ω. Note the symmetry with respect to the real axis, owing to complex conjugation $b_\pm(-\omega) = \overline{b_\pm(\omega)}$. Unstable dimensions are indicated by $(E(b))$. Note $E(b) = 0$ inside the shaded loop Λ_a. Parameter: $a = 0.1$.

As $E_\pm \geq 0$ and $E_+(0) = 2, E_-(0) = 0$ we study the changes of $E_+(b)$ via $\eta = i\tilde{\omega}$, first, hoping for a region of $b \in \mathbb{C}$ where $E(b) = 0$. Solving equation (5.3a) with

$$\eta = i\tilde{\omega} = i(1 + 2\omega), \tag{5.9}$$

we obtain the Hopf curves

$$b = b_+(\omega) = 2\frac{a - i\omega}{1 + \exp(-2\pi i\omega)} = a + \omega\tan(\pi\omega) + i(-\omega + a\tan(\pi\omega)) \tag{5.10}$$

with singularities at odd integers 2ω. See the solid lines of figure 5 for a sketch of these Hopf curves, when $a = 0.1$.

Solving equation (5.3b) with $\eta = i\tilde{\omega} = i(1 + 2\omega)$, we obtain the Hopf curves

$$b = b_-(\omega) = 2\frac{i\omega}{\exp(-2\pi i\omega) - 1} = -\omega(\cot(\pi\omega) + i) \tag{5.11}$$

with singularities at integer $\omega \neq 0$. See the dashed lines of figure 5. Note how these dashed lines correspond to the solid lines of figure 4 because equation (5.11) corresponds to equation (4.8) in the sense that $b_-(\omega) = 2b(\omega)$.

To determine the changes of the real unstable dimensions $E(b) = E_+(b) + E_-(b)$ along the curves $\omega \mapsto b_\pm(\omega)$, we observe that the zeros of $\chi_\pm$ are given as complex analytic functions. An elementary calculation shows that the complex derivative $b'_-(\omega)$ never vanishes and hence implicit differentiation applies to the Hopf curve. The complex derivative $b'_+(\omega)$ vanishes if and only if

$$a = \frac{1}{\pi} \quad \text{and} \quad \omega = 0. \tag{5.12}$$

This is precisely where the shaded loop Λ_a of figure 5 is formed. For

$$0 < a < \frac{1}{\pi}, \tag{5.13}$$

this loop stretches over the real interval

$$a < b < b_*(a), \tag{5.14}$$

where $b_*(a) = b_+(\omega_*(a)) > 0$ is given by equation (5.10) evaluated at the first positive solution $\omega_* = \omega_*(a) > 0$ of the transcendental equation

$$0 = \mathrm{Im}(b_+(\omega_*)) = -\omega_* + a\tan(\pi\omega_*). \tag{5.15}$$

To determine $E(b)$ in figure 5, we proceed as for figure 4. Complex analytical maps like $\omega \mapsto b_\pm(\omega)$, with non-vanishing derivatives, preserve orientation. Instability $E(b) = E_+(b) + E_-(b)$ tracks eigenvalues $Re\,\eta > 0$, i.e. η to the right of the imaginary axis $\eta = i\tilde{\omega} = i(1 + 2\omega)$. (The only zero eigenvalue $\eta = 0$ at $\omega = -1/2$ of $b_-(-1/2) = i/2$ noted in equation (5.6) makes no exception here.) Therefore, $E(b)$ is larger by two on the right side of any of the oriented curves $\omega \mapsto b = b_\pm(\omega)$, when compared with the left side. Elsewhere, $E(b)$ does not change. Starting from $E(0) = 2$, as noted in equation (5.4), it is therefore elementary to derive all strict real unstable dimensions $E(b)$ of the Hopf bifurcation point $\lambda = 2a$, as given in figure 5.

In particular, $E(b) = 0$ if and only if b is inside the shaded loop Λ_a of figure 5, and that the stabilizing loop exists if and only if $0 < a < 1/\pi$.

6. Proof of stabilization theorems

Based on the analysis of the strict unstable dimension $E(b)$ at the anti-phase Hopf bifurcation $\lambda = 2a, \tau = \pi, \eta = i$ as given in the previous section, we now proceed to prove local non-invasive delayed feedback stabilization of the bifurcating anti-phase periodic solutions, as claimed in theorems 3.1 and 3.2 for the supercritical and subcritical cases, respectively. Both proofs are based on the strategy of §4. The stabilization region $E(b) = 0$ of figure 4 for the complex control $b \in \mathbb{C}$ now has to be replaced by the shaded loop region Λ_a of $E(b) = 0$ derived in figure 2 and, in further detail, in figure 5. We recall that the loop Λ_a is bounded by the section $|\omega| \le \omega_*$ of the curve

$$b_+(\omega) = a + \omega\tan(\pi\omega) + i(-\omega + a\tan(\pi\omega)), \tag{6.1}$$

where $\omega_* = \omega_*(a)$ is the first positive solution of

$$0 = \omega_* - a\tan(\pi\omega_*). \tag{6.2}$$

See equations (5.10) and (5.15). We denote $b_*(a) := b_+(\omega_*(a)) > 0$, as above.

Analogous to §4, figure 3, we now seek the geometric situation of figure 6 for the tangents and unstable dimensions of the solid oriented Hopf curve $(\lambda(\omega), \tau(\omega))$ and the dashed curve $\tau = p_-(\lambda)/2$ of bifurcating periodic solutions. We calculate their tangents at $\lambda = 2a, \tau = \pi, \eta = i$ next; see also equation (4.9) versus equations (4.10).

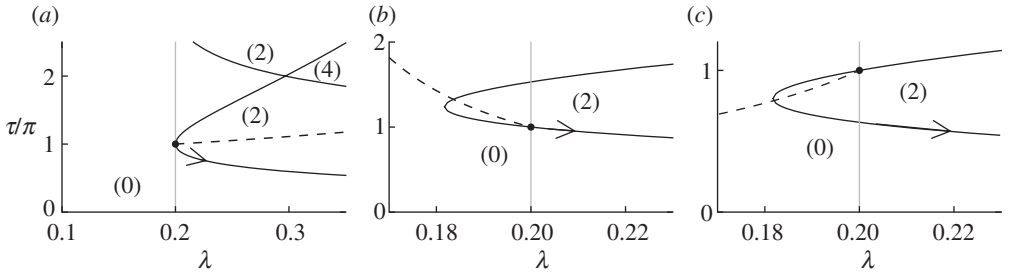

Figure 6. Anti-phase Hopf bifurcation in the parameter plane (λ, τ) for fixed control b. Solid line: Hopf bifurcation curve $(\lambda(\omega), \tau(\omega))$ through $\lambda = 0$ and non-invasive delay $\tau = \pi$. Dashed line $\tau = (1/2)p_-(\lambda)$: Pyragas curve of bifurcating periodic solutions. (a) Supercritical case $Re\,\gamma < 0$ and $a < b < b_*(a) := b_+(\omega_*(a))$; (b) subcritical soft spring case $Re\,\gamma > 0, \mathrm{Im}\,\gamma < 0$; (c) subcritical hard spring case $Re\,\gamma > 0, \mathrm{Im}\,\gamma > 0$. Parameters: (a) $Re\,\gamma = -1, \mathrm{Im}\,\gamma = -1, b = 1.0$ $(b_* \approx 1.92)$; (b) $Re\,\gamma = +1, \mathrm{Im}\,\gamma = -10, b = 0.24\,\mathrm{e}^{+\mathrm{i}\pi/8}$; (c) $Re\,\gamma = +1, \mathrm{Im}\,\gamma = +10, b = 0.24\,\mathrm{e}^{-\mathrm{i}\pi/8}$; $a = 0.1$ in all plots.

Linearizing the explicit representation

$$\tau = \frac{1}{2}p_-(\lambda) = \frac{\pi}{1 - (\lambda - 2a)\mathrm{Im}\,\gamma / Re\,\gamma} \tag{6.3}$$

of equations (2.10), (2.11) and (3.6) at $\lambda = 2a, \tau = \pi$ with $\lambda = 2a + \hat{\lambda}, \tau = \pi + \hat{\tau}$, we obtain

$$\hat{\tau} = \pi \frac{\mathrm{Im}\,\gamma}{Re\,\gamma}\hat{\lambda} \tag{6.4}$$

for the tangent to the anti-phase periodics, in analogy to equation (4.9). Analogous to equations (4.10), we also linearize the characteristic equation (5.2b), for fixed b, and obtain $0 = \chi_-(\eta) = \tilde{\lambda} - b(2\pi i\omega + i\tilde{\tau}) - 2i\omega$ with $\eta = i(1 + 2\omega)$, $\lambda = 2a + \tilde{\lambda}$, $\tau = \pi + \tilde{\tau}$. This yields the tangent to the anti-phase Hopf curve

$$\tilde{\lambda} = \frac{\mathrm{Im}\,b}{Re\,b}2\omega \tag{6.5a}$$

and

$$\tilde{\tau} = -\frac{1 + \pi\,Re\,b}{Re\,b}2\omega. \tag{6.5b}$$

We now address the supercritical case $Re\,\gamma < 0$ of theorem 3.1. In §5, we have seen how the stabilizing loop Λ_a arises for $0 < a < 1/\pi$; see assumption (3.4). We claim that all real controls b in Λ_a stabilize the local anti-phase branch of periodic solutions, i.e. all $a < b < b_*(a)$; see equation (3.5) and the explicit representation of $b_*(a)$ in equations (5.14) and (5.15) as well as equations (6.1) and (6.2). Analyticity, strict monotonicity and the claimed limits of $b_*(a)$ are obvious.

To prove stabilization, note that the slope of the anti-phase Hopf curve (6.5) is vertical in the (λ, τ) plane, for $\mathrm{Im}\,b = 0$. Moreover, the orientation is downwards, decreasing $\tilde{\tau}$, as $Re\,b > 0$ in the loop Λ_a. It remains to prove $E = 2$

along any periodic curve emanating to the supercritical right of the τ-axis, and stabilization of the bifurcating anti-phase periodic orbits will follow, as claimed in theorem 3.1.

To determine the regions $E=2$, we proceed as in §4, equations (4.13)–(4.15) but with modified real linear maps

$$\varphi(\check{\lambda},\check{\tau}) = \check{\lambda} + \eta b\, \mathrm{e}^{-\tau\eta}\check{\tau} = \check{\zeta} \tag{6.6a}$$

and

$$\psi(\check{\eta}) = (1 - \tau b\, \mathrm{e}^{-\tau\eta})\check{\eta} = \check{\zeta}, \tag{6.6b}$$

which arise from the modified characteristic equation (5.2b) for $\chi_-(\eta)=0$, replacing equation (4.7). Again

$$(\check{\lambda},\check{\tau}) = (\varphi^{-1}\circ\psi)(\check{\eta}), \tag{6.7}$$

where ψ preserves real orientation. At the point of interest $\eta = i\tilde{\omega}$, $\tilde{\omega}=1$, $\lambda=0$ and $\tau=\pi$ this time, the linear map $\varphi:\mathbb{R}^2\to\mathbb{C}\cong\mathbb{R}^2$ again possesses determinant

$$\begin{aligned}\det\varphi &= +\mathrm{Im}(\eta b\, \mathrm{e}^{-\tau\eta})\\ &= +\tilde{\omega}(Re(b)\cos(\tilde{\omega}\tau) + \mathrm{Im}\,(b)\sin(\tilde{\omega}\tau))\\ &= -Re\, b,\end{aligned} \tag{6.8}$$

because $\tilde{\omega}\tau=\pi$, this time. As $Re\, b>0$ in the loop Λ_a of linear in-phase stabilization of figure 4, the map φ *reverses* orientation, this time, and so does the composition $\varphi^{-1}\circ\psi$ of equation (6.7). Therefore, the region $E=2$ now appears *to the left* of the Hopf curve in the (λ,τ) plane. As the Hopf curve is oriented vertically downwards, the $E=2$ region contains the tangent of any supercritical Pyragas curve $\tau=(1/2)p_-(\lambda)$ emanating to the right of the τ-axis; see figure 6a. This proves theorem 3.1.

Finally, we settle the subcritical case $Re\,\gamma>0$ of theorem 3.2. Fix $0<a<1/\pi$ and consider strictly complex b in the stability loop Λ_a of figure 5, first in the soft spring case

$$\mathrm{Im}\,\gamma < 0. \tag{6.9}$$

We determine those $\mathrm{Im}\,\gamma$ next, for which such choices of b are able to stabilize the local bifurcating anti-phase branch, non-invasively. From the orientation analysis of equations (6.6)–(6.8), we again conclude $E=2$ to the left of the oriented Hopf curve in the (λ,τ) plane. Analogous to equation (4.15), it is therefore immediate that we encounter the stabilizing soft spring geometric situation of figure 6b, if and only if the Hopf slope $\tilde{\tau}/\tilde{\lambda}$ of equations (6.5) exceeds the slope $\hat{\tau}/\hat{\lambda}$ of the periodics (6.4), i.e.

$$0 > -\pi\frac{Re\, b + 1/\pi}{\mathrm{Im}\, b} > \pi\frac{\mathrm{Im}\,\gamma}{Re\,\gamma}. \tag{6.10}$$

In particular, $\mathrm{Im}\, b$ is required to be positive for the proper orientation of the Hopf curve. The least restrictive choice is given by $\Lambda_a \ni b\to b_0(a)$ defined

such that the minimum

$$\beta(a) = \min\left\{ \frac{Re\, b + 1/\pi}{\operatorname{Im} b} \,\middle|\, b \in \Lambda_a,\ \operatorname{Im} b > 0 \right\} \tag{6.11}$$

over the closure of the upper half loop $\Lambda_a \cap \{\operatorname{Im} b > 0\}$ is attained, at complex $b = b_0(a)$. Note that $b_0(a)$ is the tangent point where straight lines through $b = -1/\pi \in \mathbb{C}$ touch the boundary of the upper half of the stabilizing loop Λ_a (figure 2). This allows us to stabilize the local anti-phase branch for all subcritical soft spring γ such that

$$0 < \beta(a)\, Re\, \gamma < |\operatorname{Im} \gamma|. \tag{6.12}$$

It is completely analogous to consider stabilization in the subcritical hard spring case $Re\, \gamma > 0, 0 < a < 1/\pi$, where

$$\operatorname{Im} \gamma > 0. \tag{6.13}$$

We then arrive at the stabilizing geometric situation of figure 6*b*, for slopes

$$0 < -\pi \frac{Re\, b + 1/\pi}{\operatorname{Im} b} < \pi \frac{\operatorname{Im} \gamma}{Re\, \gamma} \tag{6.14}$$

and suitable b in the lower half loop $\Lambda_a \cap \{\operatorname{Im} b < 0\}$, again if and only if equation (6.12) holds. Indeed, the symmetry $b_+(-\omega) = \overline{b_+(\omega)}$ of the loop Λ_a implies

$$\beta(a) = \min\left\{ \frac{Re\, b + 1/\pi}{\operatorname{Im} b} \,\middle|\, b \in \Lambda_a,\ \operatorname{Im} b > 0 \right\} \tag{6.15a}$$

and

$$= \min\left\{ -\frac{Re\, b + 1/\pi}{\operatorname{Im} b} \,\middle|\, b \in \Lambda_a,\ \operatorname{Im} b < 0 \right\}. \tag{6.15b}$$

Equation (6.12) therefore allows us to locally stabilize the supercritical anti-phase branch for both the soft and hard spring cases, as was claimed in equation (3.7).

We conclude with deriving the claimed monotonicity and continuity of the minimum function $\beta(a)$ (figure 7). It is sufficient to show that the loops Λ_a strictly shrink with increasing a. Then, the maximum slopes $1/\beta(a)$ of straight lines through $b = -1/\pi \in \mathbb{C}$ and points of $\Lambda_a \cap \{\operatorname{Im} b > 0\}$ likewise decrease.

To show that the loops Λ_a strictly shrink with increasing a, we consider the map

$$(\omega, a) \longmapsto (Re\, b_+(\omega), \operatorname{Im} b_+(\omega)), \tag{6.16}$$

which defines the boundary of the loop Λ_a for $0 \le \omega \le \omega_*(a) < 1/2$; see equations (6.1) and (6.2). It is easy to check that the map (6.16) is an orientation preserving local diffeomorphism on $0 \le a < 1/\pi$, $|\omega| < 1/2$. With the given counterclockwise orientation of each loop boundary, by ω, this shows that the loops Λ_a shrink to $b = 1/\pi$ for $a \nearrow 1/\pi$. This completes the proof of theorems 3.1 and 3.2.

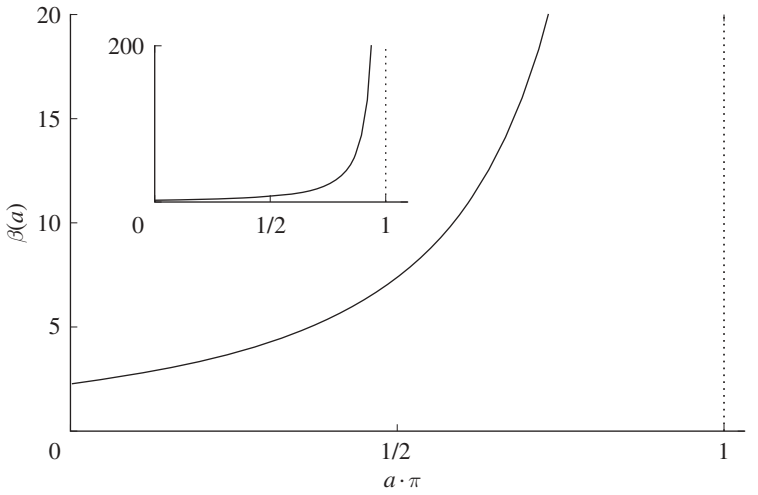

Figure 7. $\beta(a)$ is plotted (see equations (6.15)). The inset shows the function in a wider range. Note that β is monotonically increasing and $\beta(0) > 0$.

7. Numerical illustrations

In this section, we present some numerical results. Figure 8 explains the stabilization of the anti-phase orbit for the subcritical case by looking at all rotating waves (circular orbits) present in the system. The radii of rotating waves within the anti-phase manifold are plotted. The target orbit is stabilized through a transcritical bifurcation with a delay-induced rotating wave. For feedback strength a little above the stabilization, the trivial equilibrium looses its stability in a subcritical Hopf bifurcation. In the limit $\lambda \to 2a$, the Hopf bifurcation and the transcritical bifurcation occur at the same coupling strengths b_0 resulting in an instant exchange of stability.

Figure 9 displays exemplary time series for the stabilized anti-phase circular orbit in the subcritical case. When the target circular orbit is stabilized, the control signal vanishes, demonstrating the non-invasiveness of the method.

Figure 10 illustrates how the stabilization fails if condition (3.7) $|\mathrm{Im}\,\gamma| > \beta(a)\,Re\,\gamma$ is not satisfied. In this case, we have chosen $\gamma = 1 - 4i$. As $\beta(0.1) \approx 4.37$, the choice of γ slightly violates the inequality and leads to amplitude death instead of stabilized anti-phase orbits.

8. Discussion

The in-phase orbits are stable and unstable for the super- and subcritical case, respectively. As the dynamics in the flow-invariant in-phase plane is equivalent to the dynamics of a single planar system, the stabilization of the in-phase orbit in the subcritical case reduces to the stabilization of an orbit born in a planar subcritical Hopf bifurcation by delayed feedback which has previously been demonstrated (Fiedler *et al.* 2007).

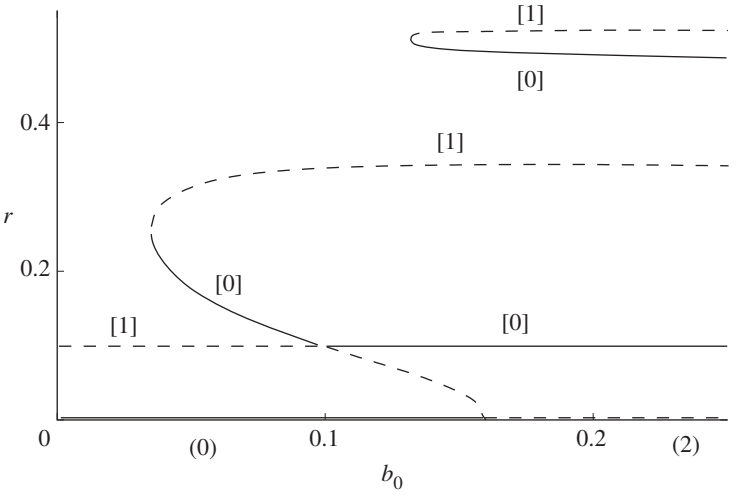

Figure 8. Stabilization of the anti-phase branch in the subcritical case. The radii of circular orbits versus the feedback gain b_0 within the anti-phase manifold are plotted; solid and dashed lines correspond to dynamically stable and unstable circular orbits, respectively. For increasing feedback strengths, b_0, a pair of stable and unstable orbits is born in a saddle–node bifurcation ($b_0 \approx 0.03$). The stable sibling then stabilizes the target orbit in a transcritical bifurcation at ($b_0 \approx 0.1$) and subsequently, having lost its stability, destabilizes the trivial equilibrium $r = 0$ in a subcritical Hopf bifurcation ($b_0 \approx 0.17$). Note that the control is non-invasive on the target orbit, i.e. not changing its radius. With further increase of feedback strengths, there is a cascade of saddle–node bifurcations generating new feedback-induced circular orbits. One of these bifurcations is shown ($b_0 \approx 0.14$). Unstable dimensions are indicated in parentheses, for the trivial equilibrium $z \equiv 0$, and in brackets, for the bifurcating periodic orbits. Parameters: $a = 0.1$, $\lambda = 2a - 0.01$, $\gamma = 1 - 10i$, $\tau = p_-/2 = \pi/(1 - (\lambda - 2a)\mathrm{Im}\,\gamma/Re\,\gamma)$, $b = b_0\,\mathrm{e}^{\mathrm{i}\pi/8}$.

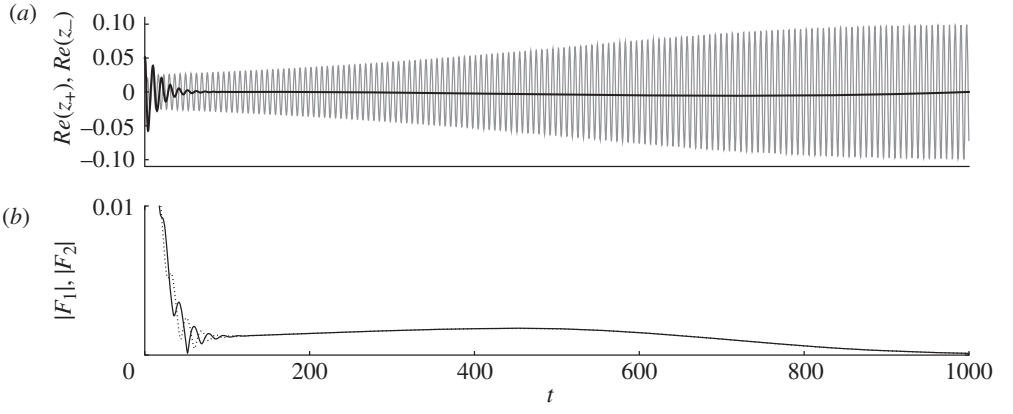

Figure 9. Stabilization of the anti-phase branch in the subcritical case. (a) Time series of $Re\,z_+$ (black) and $Re\,z_-$ (grey); (b) time series of coupling forces $F_1 := b \cdot (z_1(t-\tau) + z_2)$ (solid) and $F_2 := b \cdot (z_2(t-\tau) + z_1)$ (dotted) acting on the systems. The system starts away from the anti-phase plane $z_+ = 0$. After a short time, the in-phase component z_+ decays and the system goes to the anti-phase plane. After a longer transient, the system approaches the stabilized anti-phase orbit. Once the anti-phase orbit is reached, the control forces vanish. Parameters: $a = 0.1$, $\lambda = 2a - 0.01$, $\gamma = 1 - 10i$, $\tau = p_-/2 = \pi/(1 - (\lambda - 2a)\mathrm{Im}\,\gamma/Re\,\gamma)$, $b = 0.24\,\mathrm{e}^{\mathrm{i}\pi/8}$.

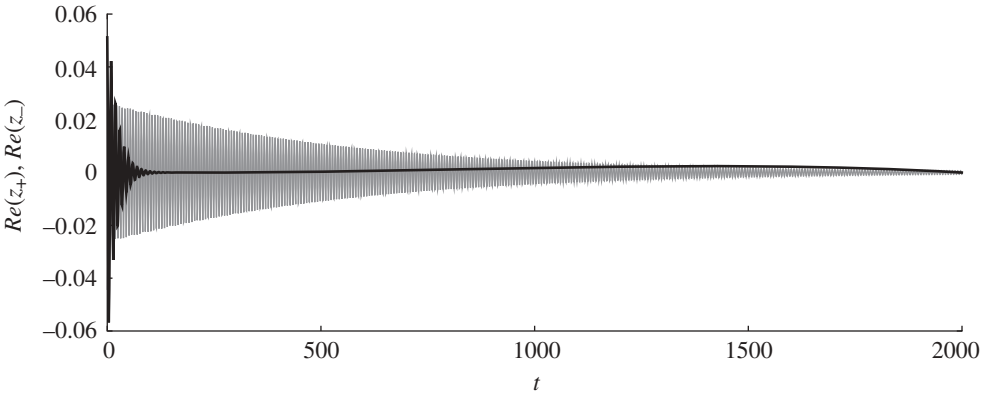

Figure 10. The time series of $Re\, z_+$ (black) and $Re\, z_-$ (grey) is plotted for the same parameters as in figure 9 except $\gamma = 1 - 4i$. This γ violates condition (3.7) and fails to stabilize the anti-phase circular orbit. Instead, the feedback system dies out to its trivial equilibrium $z_+ = z_- = 0$.

Now, we are also able to stabilize unstable anti-phase orbits in certain combinations of super-/subcritical and soft/hard spring cases. Stabilization is achieved locally near Hopf bifurcation. In the supercritical case of two unstable Floquet multipliers, real feedback gains were sufficient, both for soft and for hard springs. In the subcritical case of three unstable Floquet multipliers, by contrast, stabilization could only be achieved by complex feedback gains and for sufficiently nonlinear (soft or hard) springs. The crucial limitation $|\mathrm{Im}\,\gamma| > \beta(a)\, Re\,\gamma$ was derived in equation (3.7). Here, $|\mathrm{Im}\,\gamma|$ measures the dependence of the minimal period of the individual oscillator upon amplitude, $Re\,\gamma > 0$ measures the subcriticality of the Hopf bifurcation and a is the strength of diffusive coupling. The coupling strength was limited to $0 < a < 1/\pi$, where π corresponds to the normalized half period at anti-phase Hopf bifurcation.

9. Conclusion

In conclusion, we have studied two identical, diffusively coupled Hopf normal form oscillators of both super- and subcritical type. By introducing a delay coupling of half the minimal period, we are able to non-invasively stabilize anti-phase orbits of the coupled systems, which are inherently unstable. We prove stabilization theorems for the hard spring case and sketch the similar proof for the soft spring case.

10. Outlook

Building on this work, it will be interesting to apply our method to stabilize anti-phase orbits in physical and biological systems such as coupled lasers and coupled neurons. From a mathematical point of view generalizations to n oscillators and thus n-fold symmetries may be an interesting direction to pursue (D'Huys *et al.* 2008; Choe *et al.* submitted). For the Pyragas control scheme Q2 of planar in-phase circular orbits, it has been shown (Fiedler 2008) that only

orbits whose real Floquet multipliers μ obey $\mu < \exp(2.7)$ can be stabilized. Similar Floquet constraints may apply for our control scheme. Although we believe our non-invasive stabilization strategy to be well adapted to anti-phase periodic oscillations, only the derivation and comparison of such fundamental constraints will settle our quest for efficient non-invasive feedback stabilization of spatio-temporal patterns.

This work was supported by Deutsche Forschungsgemeinschaft in the framework of Sfb 555.

References

Baba, N., Amann, A., Schöll, E. & Just, W. 2002 Giant improvement of time-delayed feedback control by spatio-temporal filtering. *Phys. Rev. Lett.* **89**, 074101. (doi:10.1103/PhysRevLett.89.074101)

Beck, O., Amann, A., Schöll, E., Socolar, J. E. S. & Just, W. 2002 Comparison of time-delayed feedback schemes for spatio-temporal control of chaos in a reaction–diffusion system with global coupling. *Phys. Rev. E* **66**, 016213. (doi:10.1103/PhysRevE.66.016213)

Boccaletti, S., Grebogi, C., Lai, Y. C., Mancini, H. & Maza, D. 2000 The control of chaos: theory and applications. *Phys. Rep.* **329**, 103. (doi:10.1016/S0370-1573(99)00096-4)

Choe, C.-U., Dahms, T., Hövel, P. & Schöll, E. Submitted. Controlling splay and cluster states by delay coupling in networks. (http://arXiv:0908.3984).

Dahlem, M. A., Schneider, F. M. & Schöll, E. 2008 Failure of feedback as a putative common mechanism of spreading depolarizations in migraine and stroke. *Chaos* **18**, 026110. (doi:10.1063/1.2937120)

Dahlem, M. A., Hiller, G., Panchuk, A. & Schöll, E. 2009 Dynamics of delay-coupled excitable neural systems. *Int. J. Bifur. Chaos* **19**, 745. (doi:10.1142/S0218127409023111)

Dahlem, M. A., Graf, R., Strong, A. J., Dreier, J. P., Dahlem, Y. A., Sieber, M., Hanke, W., Podoll, K. & Schöll, E. In press. Two-dimensional wave patterns of spreading depolarization: retracting, re-entrant, and stationary waves. *Physica D.*

Dahms, T., Hövel, P. & Schöll, E. 2007 Control of unstable steady states by extended time-delayed feedback. *Phys. Rev. E* **76**, 056201. (doi:10.1103/PhysRevE.76.056201)

Dahms, T., Hövel, P. & Schöll, E. 2008 Stabilizing continuous-wave output in semiconductor lasers by time-delayed feedback. *Phys. Rev. E* **78**, 056213. (doi:10.1103/PhysRevE.78.056213)

D'Huys, O., Vicente, R., Erneux, T., Danckaert, J. & Fischer, I. 2008 Synchronization properties of network motifs: influence of coupling delay and symmetry. *Chaos* **18**, 037116. (doi:10.1063/1.2953582)

Diekmann, O., van Gils, S. A., Verduyn Lunel, S. M. & Walther, H. O. 1995 *Delay equations.* New York, NY: Springer-Verlag.

Fiedler, B. 2008 Time-delayed feedback control: qualitative promise and quantitative constraints. In *Proc. 6th EUROMECH non-linear dynamics Conf.* (*ENOC-2008*) (eds A. Fradkov & B. Andrievsky). See http://lib.physcon.ru/?item=1568.

Fiedler, B., Flunkert, V., Georgi, M., Hövel, P. & Schöll, E. 2007 Refuting the odd number limitation of time-delayed feedback control. *Phys. Rev. Lett.* **98**, 114101. (doi:10.1103/PhysRevLett.98.114101)

Fiedler, B., Flunkert, V., Georgi, M., Hövel, P. & Schöll, E. 2008 Beyond the odd number limitation of time-delayed feedback control. In *Handbook of chaos control* (eds E. Schöll & H. G. Schuster), pp. 73–84, 2nd completely revised and enlarged edn. Weinheim, Germany: Wiley-VCH.

Fiedler, B., Flunkert, V., Georgi, M., Hövel, P. & Schöll, E. 2008 Delay stabilization of rotating waves without odd number limitation. In *Reviews of nonlinear dynamics and complexity*, vol. 1 (ed. H. G. Schuster), pp. 53–68. Weinheim, Germany: Wiley-VCH.

Fiedler, B., Yanchuk, S., Flunkert, V., Hövel, P. Wünsche, H. J. & Schöll, E. 2008 Delay stabilization of rotating waves near fold bifurcation and application to all-optical control of a semiconductor laser. *Phys. Rev. E* **77**, 066207. (doi:10.1103/PhysRevE.77.066207)

Fischer, I., Vicente, R., Buldú, J. M., Peil, M., Mirasso, C. R., Torrent, M. C. & García-Ojalvo, J. 2006 Zero-lag long-range synchronization via dynamical relaying. *Phys. Rev. Lett.* **97**, 123902. (doi:10.1103/PhysRevLett.97.123902)

Flunkert, V. & Schöll, E. 2007 Suppressing noise-induced intensity pulsations in semiconductor lasers by means of time-delayed feedback. *Phys. Rev. E* **76**, 066202. (doi:10.1103/PhysRevE.76.066202)

Flunkert, V., D'Huys, O., Danckaert, J., Fischer, I. & Schöll, E. 2009 Bubbling in delay-coupled lasers. *Phys. Rev. E* **79**, 065201.

Gassel, M., Glatt, E. & Kaiser, F. 2007 Time-delayed feedback in a net of neural elements: transitions from oscillatory to excitable dynamics. *Fluct. Noise Lett.* **7**, L225. (doi:10.1142/S0219477507003878)

Gauthier, D. J. 2003 Resource letter: controlling chaos. *Am. J. Phys.* **71**, 750. (doi:10.1119/1.1572488)

Harrington, I. & Socolar, J. E. S. 2001 Limitation on stabilizing plane waves via time-delay feedback. *Phys. Rev. E* **64**, 056206. (doi:10.1103/PhysRevE.64.056206)

Hauschildt, B., Janson, N. B., Balanov, A. G. & Schöll, E. 2006 Noise-induced cooperative dynamics and its control in coupled neuron models. *Phys. Rev.* E **74**, 051906. (doi:10.1103/PhysRevE.74.051906)

Hizanidis, J. & Schöll, E. 2008 Control of coherence resonance in semiconductor superlattices. *Phys. Rev. E* **78**, 066205. (doi:10.1103/PhysRevE.78.066205)

Hövel, P. & Schöll, E. 2005 Control of unstable steady states by time-delayed feedback methods. *Phys. Rev. E* **72**, 046203. (doi:10.1103/PhysRevE.72.046203)

Janson, N. B., Balanov, A. G. & Schöll, E. 2004 Delayed feedback as a means of control of noise-induced motion. *Phys. Rev. Lett.* **93**, 010601. (doi:10.1103/PhysRevLett.93.010601)

Just, W., Bernard, T., Ostheimer, M., Reibold, E. & Benner, H. 1997 Mechanism of time-delayed feedback control. *Phys. Rev. Lett.* **78**, 203. (doi:10.1103/PhysRevLett.78.203)

Just, W., Fiedler, B., Flunkert, V., Georgi, M., Hövel, P. & Schöll, E. 2007 Beyond odd number limitation: a bifurcation analysis of time-delayed feedback control. *Phys. Rev. E* **76**, 026210. (doi:10.1103/PhysRevE.76.026210)

Kehrt, M., Hövel, P. Flunkert, V., Dahlem, M. A., Rodin, P. & Schöll, E. 2009 Stabilization of complex spatio-temporal dynamics near a subcritical Hopf bifurcation by time-delayed feedback. *Eur. Phys. J. B* **68**, 557. (doi:10.1140/epjb/e2009-00132-5)

Klein, E., Gross, N., Rosenbluh, M., Kinzel, W., Khaykovich, L. & Kanter, I. 2006 Stable isochronal synchronization of mutually coupled chaotic lasers. *Phys. Rev. E* **73**, 066214. (doi:10.1103/PhysRevE.73.066214)

Kyrychko, Y. N., Blyuss, K. B., Hogan, S. J. & Schöll, E. Submitted. Control of spatio-temporal patterns in the Gray–Scott model. *Chaos.* **Q4**

Landsman, A. S. & Schwartz, I. B. 2007 Complete chaotic synchronization in mutually coupled time-delay systems. *Phys. Rev. E* **75**, 026201. (doi:10.1103/PhysRevE.75.026201)

Majer, N. & Schöll, E. 2009 Resonant control of stochastic spatio-temporal dynamics in a tunnel diode by multiple time delayed feedback. *Phys. Rev. E* **79**, 011109. (doi:10.1103/PhysRevE.79.011109)

Nakajima, H. 1997 On analytical properties of delayed feedback control of chaos. *Phys. Lett. A* **232**, 207. (doi:10.1016/S0375-9601(97)00362-9)

Nakajima, H. & Ueda, Y. 1998 Limitation of generalized delayed feedback control. *Physica D* **111**, 143. (doi:10.1016/S0167-2789(97)80009-7)

Nakajima, H. & Ueda, Y. 1998 Half-period delayed feedback control for dynamical systems with symmetries. *Phys. Rev. E* **58**, 1757. (doi:10.1103/PhysRevE.58.1757)

Ott, E., Grebogi, C. & Yorke, J. A. 1990 Controlling chaos. *Phys. Rev. Lett.* **64**, 1196. (doi:10.1103/PhysRevLett.64.1196)

Pomplun, J., Amann, A. & Schöll, E. 2005 Mean field approximation of time-delayed feedback control of noise-induced oscillations in the Van der Pol system. *Europhys. Lett.* **71**, 366. (doi:10.1209/epl/i2005-10100-9)

Popovych, O. V., Hauptmann, C. & Tass, P. A. 2005 Effective desynchronization by nonlinear delayed feedback. *Phys. Rev. Lett.* **94**, 164102. (doi:10.1103/PhysRevLett.94.164102)

Postlethwaite, C. M. & Silber, M. 2007 Spatial and temporal feedback control of traveling wave solutions of the two-dimensional complex Ginzburg–Landau equation. *Physica D* **236**, 65. (doi:10.1016/j.physd.2007.07.011)

Pototsky, A. & Janson, N. B. 2007 Correlation theory of delayed feedback in stochastic systems below Andronov Hopf bifurcation. *Phys. Rev. E* **76**, 056208. (doi:10.1103/PhysRevE.76.056208)

Prager, T., Lerch, H. P., Schimansky-Geier, L. & Schöll, E. 2007 Increase of coherence in excitable systems by delayed feedback. *J. Phys. A* **40**, 11045. (doi:10.1088/1751-8113/40/36/005)

Pyragas, K. 1992 Continuous control of chaos by self-controlling feedback. *Phys. Lett. A* **170**, 421. (doi:10.1016/0375-9601(92)90745-8)

Pyragas, V. & Pyragas, K. 2006 Delayed feedback control of the Lorenz system: An analytical treatment at a subcritical Hopf bifurcation. *Phys. Rev. E* **73**, 036215. (doi:10.1103/PhysRevE.73.036215)

Pyragas, K., Pyragas, V. & Benner, H. 2004 Delayed feedback control of dynamical systems at subcritical Hopf bifurcation. *Phys. Rev. E* **70**, 056222. (doi:10.1103/PhysRevE.70.056222)

Rosenblum, M. G. & Pikovsky, A. 2004 Delayed feedback control of collective synchrony: An approach to suppression of pathological brain rhythms. *Phys. Rev. E* **70**, 041904. (doi:10.1103/PhysRevE.70.041904)

Rosenblum, M. G., Pikovsky, A. & Kurths, J. 2001 *Synchronization—a universal concept in nonlinear sciences.* Cambridge, UK: Cambridge University Press.

Schiff, S. J., Jerger, K., Duong, D. H., Chang, T., Spano, M. L. & Ditto, W. L., 1994 Controlling chaos in the brain. *Nature* **370**, 615. (doi:10.1038/370615a0)

Schikora, S., Hövel, P. Wünsche, H. J. Schöll, E. & Henneberger, F. 2006 All-optical noninvasive control of unstable steady states in a semiconductor laser. *Phys. Rev. Lett.* **97**, 213902. (doi:10.1103/PhysRevLett.97.213902)

Schneider, F. M., Schöll, E. & Dahlem, M. A. 2009 Controlling the onset of traveling pulses in excitable media by nonlocal spatial coupling and time delayed feedback. *Chaos* **19**, 015110. (doi:10.1063/1.3096411)

Schöll, E. & Pyragas, K. 1993 Tunable semiconductor oscillator based on self-control of chaos in the dynamic Hall effect. *Europhys. Lett.* **24**, 159. (doi:10.1209/0295-5075/24/3/001)

Schöll, E. & Schuster, H. G. (eds) 2008 *Handbook of chaos control*, 2nd completely revised and enlarged edn. Weinheim, Germany: Wiley-VCH.

Schöll, E., Hiller, G., Hövel, P. & Dahlem, M. A. 2009 Time-delayed feedback in neurosystems. *Phil. Trans. R. Soc. A* **367**, 1079. (doi:10.1098/rsta.2008.0258)

Shaw, L. B., Schwartz, I. B., Rogers, E. A. & Roy, R. 2006 Synchronization and time shifts of dynamical patterns for mutually delay-coupled fiber ring lasers. *Chaos* **16**, 015111. (doi:10.1063/1.2150407)

Sieber, J., Gonzalez-Buelga, A., Neild, S., Wagg, D. & Krauskopf, B. 2008 Experimental continuation of periodic orbits through a fold. *Phys. Rev. Lett.* **100**, 244101. (doi:10.1103/PhysRevLett.100.244101)

Stegemann, G., Balanov, A. G. & Schöll, E. 2006 Delayed feedback control of stochastic spatiotemporal dynamics in a resonant tunneling diode. *Phys. Rev. E* **73**, 016203. (doi:10.1103/PhysRevE.73.016203)

Unkelbach, J., Amann, A., Just, W. & Schöll, E. 2003 Time–delay autosynchronization of the spatiotemporal dynamics in resonant tunneling diodes. *Phys. Rev. E* **68**, 026204. (doi:10.1103/PhysRevE.68.026204)

von Loewenich, C., Benner, H. & Just, W. 2004 Experimental relevance of global properties of time-delayed feedback control. *Phys. Rev. Lett.* **93**, 174101. (doi:10.1103/PhysRevLett.93.174101)

Wünsche, H. J. *et al.* 2005 Synchronization of delay-coupled oscillators: a study of semiconductor lasers. *Phys. Rev. Lett.* **94**, 163901. (doi:10.1103/PhysRevLett.94.163901)